Article

Acid Leaching of Al- and Ta-Substituted Li₇La₃Zr₂O₁₂ (LLZO) Solid Electrolyte

Kirstin Schneider [1,*], Vivien Kiyek [2], Martin Finsterbusch [2,3], Bengi Yagmurlu [1] and Daniel Goldmann [1]

[1] Institute of Mineral and Water Processing, Recycling and Circular Economy Systems, Clausthal University of Technology, Walther-Nernst-Str. 9, 38678 Clausthal-Zellerfeld, Germany

[2] Institute of Energy and Climate Research—Materials Synthesis and Processing (IEK-1), Forschungszentrum Jülich GmbH, 52425 Jülich, Germany

[3] Helmholtz Institute Münster—Ionics in Energy Storage (IEK-12), Forschungszentrum Jülich GmbH, 52425 Jülich, Germany

* Correspondence: kirstin.schneider@tu-clausthal.de

Abstract: Solid-state batteries (SSBs) are promising next-generation batteries due to their potential for achieving high energy densities and improved safety compared to conventional lithium-ion batteries (LIBs) with a flammable liquid electrolyte. Despite their huge market potential, very few studies have investigated SSB recycling processes to recover and reuse critical raw metals for a circular economy. For conventional LIBs, hydrometallurgical recycling has been proven to be able to produce high-quality products, with leaching being the first unit operation. Therefore, it is essential to establish a fundamental understanding of the leaching behavior of solid electrolytes as the key component of SSBs with different lixiviants. This work investigates the leaching of the most promising Al- and Ta-substituted Li₇La₃Zr₂O₁₂ (LLZO) solid electrolytes in mineral acids (H₂SO₄ and HCl), organic acids (formic, acetic, oxalic, and citric acid), and water. The leaching experiments were conducted using actual LLZO production waste in 1 M of acid at 1:20 S/L ratio at 25 °C for 24 h. The results showed that strong acids, such as H₂SO₄, almost completely dissolved LLZO. Encouraging selective leaching properties were observed with oxalic acid and water. This fundamental knowledge of LLZO leaching behavior will provide the basis for future optimization studies to develop innovative hydrometallurgical SSB recycling processes.

Keywords: lithium-ion batteries; solid-state batteries; critical raw materials; leaching; hydrometallurgy; recycling; circular economy

1. Introduction

Electrochemical energy conversion and storage technologies are critical for energy transition to combat climate change [1,2]. Since the commercialization of lithium-ion batteries (LIBs), they have proven to be highly reliable and efficient in terms of lifetime as well as energy and power density [3,4]. Conventional LIBs with a liquid electrolyte dominate the current battery market for consumer electronics, power electronics, electric vehicles, and stationary energy storage [5,6]. However, the liquid electrolyte, consisting of lithium salts dissolved in flammable organic solvents, poses a safety risk not only during use but also during recycling due to potential thermal runaway and HF emissions [7–9]. In addition, the e-mobility industry, in particular, is striving for higher battery performance. To meet industry demands while improving safety, researchers are working on next-generation batteries, such as solid-state lithium batteries (SSBs) with solid electrolytes (SEs). SSBs offer the possibility of a significant increase in energy density with improved safety features due to the absence of a flammable liquid electrolyte.

The SE is the key component of SSBs. A promising oxide-based SE is garnet-type Li₇La₃Zr₂O₁₂ (LLZO) [10]. The advantages of LLZO are its high ionic conductivity at room temperature from 10^{-4} to 10^{-3} S cm^{-1}, its wide electrochemical window from 0 to 5 V, and

its good chemical stability against Li metal [11]. The challenges of LLZO are its limited compatibility with high-capacity NMC-class cathode active materials, the use of expensive raw materials, and the use of energy-intensive processing techniques [12]. Nevertheless, the strategic advantages outweigh the disadvantages, and the use of LLZO is being intensively researched [11,13].

In a circular economy, science-based recycling strategies for SSBs should be in place prior to their industrial implementation, ideally enabling a design-for-recycling strategy. However, SSB technologies currently under investigation present new and specific challenges for recycling. First, the cell design of oxide-based SSBs is expected to change significantly compared to conventional LIBs with a liquid electrolyte [14]. Second, oxide-based SSBs introduce new elements, such as La, Ta, and Zr, into the recycling process that are not present in current battery generations. The European Union classifies La and Ta as critical raw materials (CRMs) [15]. Therefore, the recovery and reuse of CRMs should be given a high priority. Although Zr is not yet classified as a CRM, it has been included for the first time in the 2020 assessment [15]. In addition, Li, a CRM, is not only present in conventional LIBs but also in SSBs at much higher levels [15]. For SSBs, it is, therefore, necessary to investigate whether the existing recycling concepts for conventional LIBs can remain unchanged, whether they need to be adapted, or whether new processes need to be developed.

Recycling concepts for conventional LIBs combine various process technologies, such as pyrometallurgy, mechanical processing, thermal treatment, and hydrometallurgy [16–18]. Most recycling concepts include hydrometallurgical extraction processes. This is because hydrometallurgy allows flexible and high-quality product recovery from a complex and diverse input stream, such as waste LIBs, with low energy consumption [19,20]. Leaching is the first unit operation in a hydrometallurgical process. Mineral acids are highly effective lixiviants for conventional LIBs. Sulfuric acid and hydrochloric acid are the most studied lixiviants, and high leaching efficiencies of >99% are possible when applied under optimal conditions [21–23]. In addition, organic acids are increasingly being investigated as they are considered environmentally friendly [24–26].

In contrast to conventional LIBs, there are few studies on the hydrometallurgical recycling of SSBs, especially for LLZO. According to Schwich et al., elevated temperatures and strong acids are required to leach sintered LLZO [27]. Ali Nowroozi et al. studied the leaching of $LiFePO_4/LLZO/Li_4Ti_5O_{12}$ cells using hydrochloric acid at different concentrations (5 g/L of solids, T = 80 °C, and 6 h) [28]. LLZO is leached with a low acid concentration at pH = 2. Maximum La and Zr recoveries are reported to be 82% and 87%, respectively [28]. Although this study provides valuable insights, further research is needed to understand LLZO leaching in different lixiviants.

Since leaching is the first step in a hydrometallurgical process, a holistic acid screening study is required to subsequently develop a separation and purification process. The objective is to investigate the leaching of LLZO in water compared to the most common mineral and organic acids used in conventional LIB recycling processes. In this study, the following lixiviants were selected for this purpose: sulfuric acid (H_2SO_4) and hydrochloric acid (HCl) as the mineral acids, and formic acid (HCOOH), acetic acid (CH_3COOH), oxalic acid ($C_2H_2O_4$), and citric acid ($C_6H_8O_7$) as the organic acids. These lixiviants were studied to develop flexible recycling routes with options for complete and selective LLZO dissolution.

2. Materials and Methods

2.1. Materials

2.1.1. LLZO Samples

Three Al- and Ta-substituted LLZO samples were provided by Forschungszentrum Jülich (Jülich, Germany) for the leaching experiments: two batches of calcined LLZO and one batch of sintered LLZO. The samples were obtained from a separator production

process of SSBs (see Supplementary Material S1) and were used to investigate whether calcined and sintered LLZO exhibit a different leaching behavior.

The first sample, calcined LLZO #1, was an aged material due to its temporary storage outside of a glove box. To restore its original properties, calcined LLZO #1 was thermally treated prior to leaching (see Supplementary Material S2). The second sample, calcined LLZO #2, was used immediately after collection and, therefore, did not undergo additional thermal treatment. The third sample, sintered LLZO #2, was also used immediately after collection, as was the calcined LLZO #2 sample. Both calcined LLZO samples were powders, whereas sintered LLZO #2 consisted of cylindrical pellets approximately 1 cm in diameter and of variable height (Figure S2).

2.1.2. Chemicals

Deionized water, two mineral acids, and four organic acids were evaluated for the leaching of LLZO. Deionized water was used to establish a baseline. Sulfuric acid (95–97% H_2SO_4 p.a., Honeywell Fluka, Morristown, NJ, USA), hydrochloric acid (fuming HCl $\geq$ 37%, p.a., Honeywell Fluka), acetic acid (100% p.a., Carl Roth, Karlsruhe, Germany), and formic acid (98–100% p.a., Merck, Darmstadt, Germany) were diluted with deionized water to the target concentration of 1 M. The solutions of 1 M oxalic acid and 1 M citric acid were prepared by mixing anhydrous oxalic acid ($\geq$99.0% p.a., Sigma Aldrich, St. Louis, MO, USA) and anhydrous citric acid ($\geq$99.5% p.a., Carl Roth, Karlsruhe, Germany) with the required amount of deionized water.

2.2. Methods

2.2.1. Characterization of the LLZO Samples

All three samples were characterized in terms of chemical composition, initial phase composition, and particle size distribution. The calcined LLZO samples were already available in powder form. The sintered LLZO #2 sample was dry milled in a vibratory disk mill to obtain a powder. Each sample was split using a rotary sample splitter to produce representative samples.

The chemical composition was analyzed using inductively coupled plasma optical emission spectroscopy (ICP-OES) with an Agilent 5100 ICP-OES system (Agilent Technologies Inc., Santa Clara, CA, USA). Solutions of the solid samples were prepared by microwave digestion with ammonium sulfate and concentrated sulfuric acid using a turboWAVE® system (MLS-MWS Laboratory Solutions, Leutkirch, Germany).

The initial phase composition was determined using powder X-ray diffraction (XRD) with a PANalytical X-Pert Pro diffractometer equipped with a Co X-ray tube (Malvern Panalytical, Malvern, UK).

The particle size distribution was measured using laser diffraction with a HELOS/KR system equipped with a RODOS dry dispenser (Sympatec GmbH, Clausthal-Zellerfeld, Germany). Three replicate measurements were performed, and the mean value was determined.

2.2.2. Leaching Experiments

All three samples were leached in deionized water, two mineral acids (sulfuric acid and hydrochloric acid), and four organic acids (acetic, formic, oxalic, and citric acid). The samples were weighed and vacuum-packed in bags at the beginning of the test series to avoid inhomogeneities during the experiments due to side reactions with air.

The leaching experiments were performed in a double-jacketed glass reactor (Rettberg GmbH, Göttingen, Germany). A total of 150 mL of lixiviant was added to the reactor for thermal equilibration. The reaction temperature was kept constant at 25 °C using a thermostat (N6 Circulator, Thermo HaakeTM, Thermo Fisher Scientific Inc., Waltham, MA, USA) with a PTFE-coated PT 100 temperature probe (Bohlender GmbH, Grünsfeld, Germany) immersed in the leach solution. The experiments were conducted under constant gentle stirring conditions at 400 rpm using a magnetic stirrer (Hei-Connect, Heidolph Instruments,

Schwabach, Germany). A total of 7.5 g of each sample was added to obtain a solid/liquid (S/L) ratio of 50 g/L. The reaction time was started after complete sample addition.

For chemical analysis, liquid samples were collected with an Eppendorf pipette after 3 and 24 h of leaching. The samples were diluted with deionized water and filtered with a 0.45 μm cellulose acetate syringe filter. Chemical composition was analyzed using ICP-OES with an Agilent 5100 ICP-OES system (Agilent Technologies Inc., Santa Clara, CA, USA). The elemental concentrations of the pregnant leach solutions after 24 h leaching are provided in Table S1 (see Supplementary Material S4). The leaching efficiency, $Y_{i,j,t}$, was calculated for each element i in sample j present in the leach solution after t hours according to the following equation:

$$Y_{i,j,t} = \frac{C_{i,j,t} \cdot V_L}{x_{0,i,j} \cdot m_{feed}} \cdot 100\% \tag{1}$$

where $C_{i,j,t}$ is the concentration of element i in the leach solution of sample j after t hours (in g/L); V_L is the total volume of the leach solution (in L); $x_{0,i,j}$ is the concentration of element i in the input material of sample j (in wt%); and m_{feed} is the weight of the input material (in g). The results were verified based on an analysis of the solid leaching residues. Due to the heterogeneous nature of the samples, leaching efficiencies sometimes exceeded 100% by a maximum of 5.8%.

Leaching was performed for a total of 24 h. At the end of the leaching process, the pH (pH electrode Inlab Micro, Mettler-Toledo GmbH, Columbus, OH, USA) and the redox potential (ORP electrode InLab Redox Micro, Mettler-Toledo GmbH, Columbus, OH, USA) were measured. The samples were filtered using vacuum filtration. The residues were washed with deionized water and dried in an oven at 105 °C until a constant weight was reached. A Bruker D4 Endeavor equipped with a 1D Detector LYNXEY (Bruker Corporation, Billerica, MA, USA) using monochromatized Cu Kα radiation was used for phase analysis of the leaching residues.

3. Results and Discussion

3.1. Characterization of the LLZO Samples

Two samples of calcined LLZO and one sample of sintered LLZO were used in this study. In addition to leaching LLZO with different lixiviants, it was investigated whether calcined and sintered LLZO exhibit different leaching characteristics.

The three LLZO samples had a similar chemical composition with a maximum standard deviation of 1.54 wt% for La (Table 1). As expected, the samples consisted mainly of La, Zr, Ta, and Li with less than 1 wt% Al as a dopant. The quantitative analysis of light elements in a heavy matrix is often difficult [29]. Therefore, the composition of stoichiometric Al-/Ta-substituted LLZO ($Li_{6.45}Al_{0.05}La_3Zr_{1.6}Ta_{0.4}O_{12}$) was calculated to determine whether the measured values agreed with the theoretical values (last column in Table 1). The measured and theoretical elemental contents were within a similar range, and no trend toward over- or underestimation was observed. The Al content showed the largest relative variation of all the elements measured, which could be due to Al uptake from the Al_2O_3 crucible used in the material processing [30,31]. In addition, this study was conducted using actual production waste, rather than commercially purchased LLZO. Small variations in chemical composition were, therefore, expected.

The calcined and sintered LLZO samples were prepared via solid-state synthesis with multiple calcination steps to synthesize cubic LLZO phases (see Supplementary Material S1). The XRD pattern in Figure 1 confirms that cubic LLZO is the main phase in all three samples. The phase purity of the sintered LLZO #2 sample was confirmed, while the calcined LLZO samples also contained secondary phases. For calcined LLZO #1, the main reflex of the secondary phase $La_2Zr_2O_7$ was determined. For calcined LLZO #2, there are more secondary phases present. Due to the number of reflexes in LLZO and the limitations of the XRD measurements, about 5%, the reflexes cannot be assigned to specific phases.

The possible secondary phases include the precursors La_2O_3, Ta_2O_5, and ZrO_2, as well as $LiZrO_2$ and $La(AlO_3)$.

Table 1. The chemical composition of the three samples was measured using inductively coupled plasma optical emission spectroscopy (ICP-OES). The mean value and sample standard deviation were calculated. The theoretical composition of stoichiometric Al-/Ta-substituted LLZO ($Li_{6.45}Al_{0.05}La_3Zr_{1.6}Ta_{0.4}O_{12}$) is displayed in the last column. All elements are reported in weight percentage.

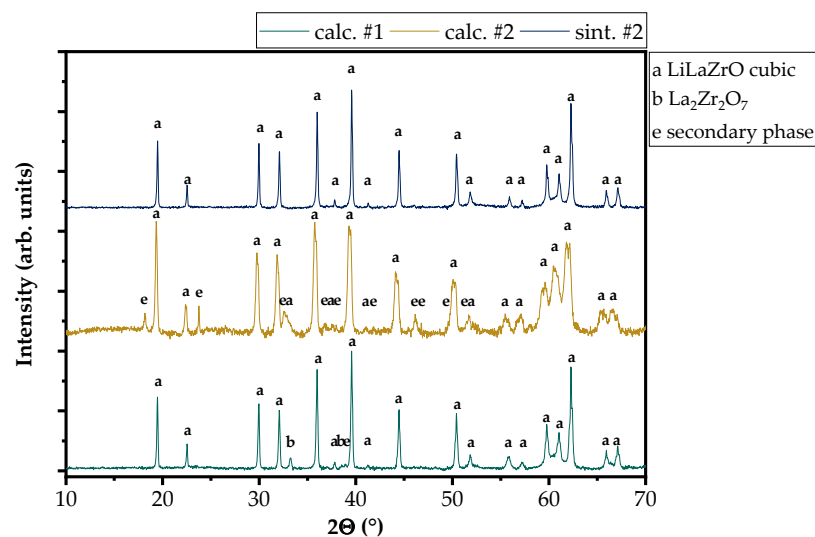| Element	Calcined LLZO #1	Calcined LLZO #2	Sintered LLZO #2	Mean Value	Sample Standard Deviation	Theoretical Composition
Li	5.76	5.19	5.42	5.46	0.29	5.13
Al	0.66	0.51	0.66	0.61	0.09	0.15
La	42.72	40.17	42.95	41.95	1.54	47.72
Zr	15.35	14.56	14.40	14.77	0.51	16.72
Ta	6.69	6.57	7.10	6.79	0.28	8.29

Figure 1. X-ray diffraction (XRD) patterns of calcined LLZO #1, calcined LLZO #2, and sintered LLZO #2. The present phases are cubic LLZO (ICSD: 182312) and $La_2Zr_2O_7$ (ICSD: 015165).

The particle size distribution of the samples was determined using laser diffraction. Calcined LLZO #1 had a homogeneous particle size distribution with an x_{50} value of 11 µm (Figure 2a). Calcined LLZO #2 had an inhomogeneous particle size distribution with two maxima (Figure 2b). In the calcined LLZO #2 sample, approximately 10% of the particles were larger than 100 µm. These particles were probably agglomerates formed by reaction with the Li precursor since the melting point of LiOH is 473 °C and, therefore, below the calcination temperature [32]. The results of the calcined LLZO samples were in agreement with the literature since as-synthesized LLZO powders typically range from 1 to 10 µm with particles up to 200 µm [33]. Due to their small particle size, the calcined LLZO samples were used for the leaching experiments without further comminution. Sintered LLZO #2 consisted of cylindrical pellets approximately 1 cm in diameter with varying heights (Figure S2). To ensure good sample comparability during leaching, the sintered LLZO #2 sample was dry milled in a vibratory disk mill to obtain a fine powder with particles less than 100 µm (Figure 2c).
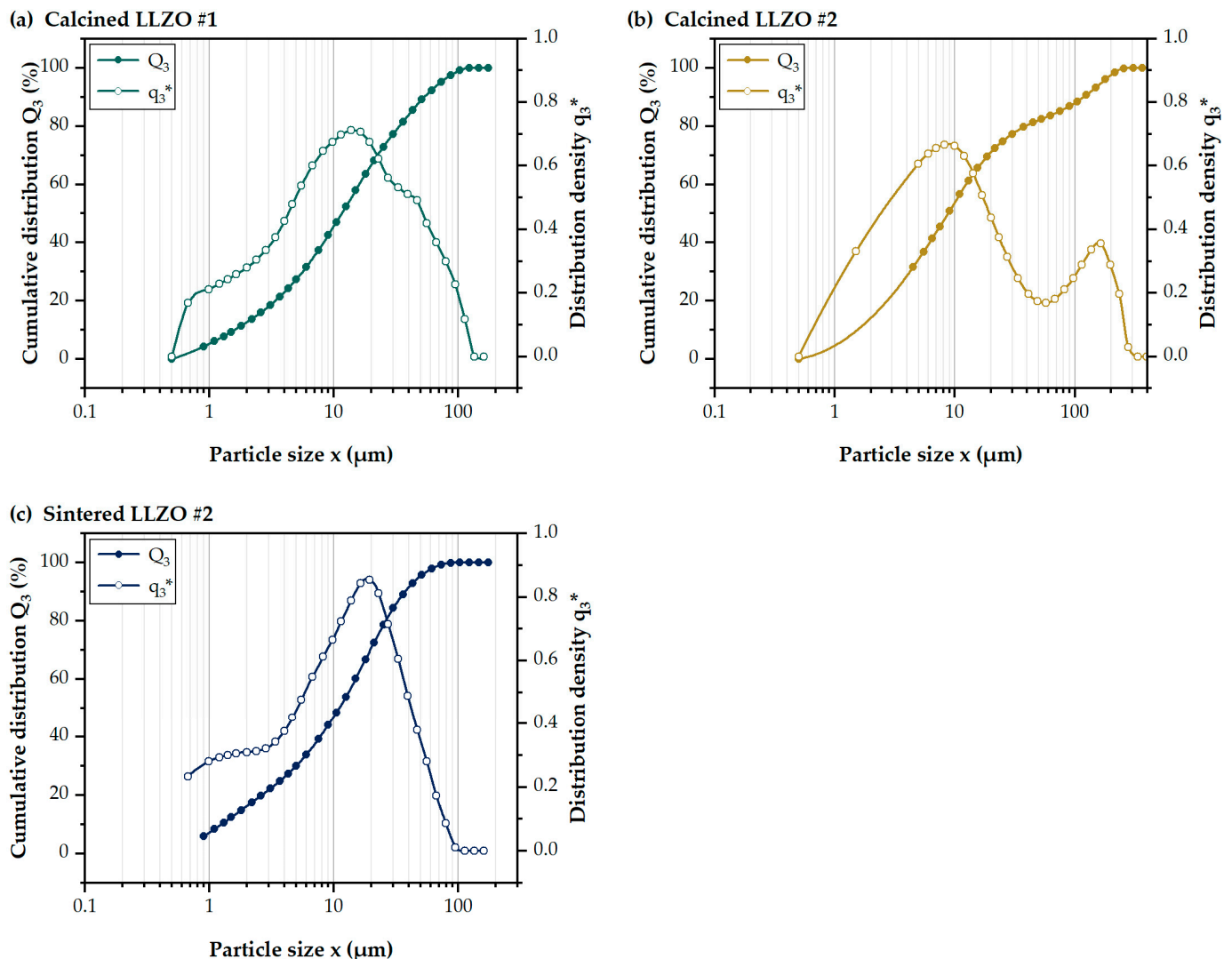
(a) Calcined LLZO #1

(b) Calcined LLZO #2

(c) Sintered LLZO #2

Figure 2. The particle size distribution of the LLZO samples used in the leaching experiments as determined by laser diffraction: calcined LLZO #1 (**a**), calcined LLZO #2 (**b**), and sintered LLZO #2 (**c**).

3.2. Leaching in Water

The most readily available and inexpensive lixiviant is water, and it must be tested before other lixiviants due to the possible presence of readily soluble metals in the LLZO samples. When LLZO was leached in deionized water, only Li and Al were detected in the leach solutions (Figure 3). As expected, the elements La, Ta, and Zr were not leached as they form more stable oxidic structures.

The Li leaching efficiency was up to 56% after 3 h, with an average increase of 6% after 24 h (Figure 3). Garnets are known to be unstable in the presence of moisture from the processing of LLZO components [33]. This instability is attributed to the Li^+/H^+ exchange reaction between garnets and water, which causes Li loss from the garnet structure and the formation of LiOH [34–37]:

$$Li_7La_3Zr_2O_{12} + x\,H_2O \rightleftharpoons Li_{7-x}H_xLa_3La_2O_{12} + x\,LiOH \tag{2}$$

The reaction kinetics of Equation (2) are fast as the pH of the solution rises rapidly from a neutral pH to 11–13 in a few minutes [38–40]. The increased pH indicates the formation of a basic LiOH solution. A proton-enriched surface layer is formed, which then inhibits further reaction of water with the inner of the particles. Therefore, a complete

Li^+/H^+ exchange does not occur. In addition, LLZO powders are expected to have higher Li leaching efficiencies than crushed LLZO pellets due to the increased surface area exposed to water [34].
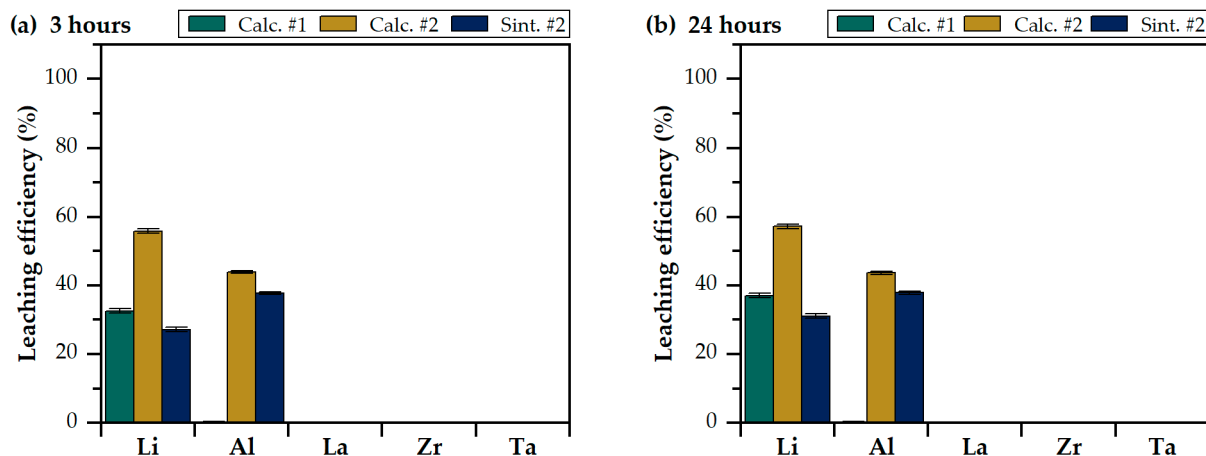

Figure 3. Leaching efficiency of the calcined and sintered LLZO samples in water after 3 h (**a**) and 24 h (**b**) (50 g/L of solids and T = 25°).

Al was leached only from calcined LLZO #2 and sintered LLZO #2 (Figure 3). No difference in leaching efficiency was observed between 3 and 24 h. It is generally accepted that Al replaces Li sites in the LLZO structure to stabilize the cubic LLZO phase [41]. However, inhomogeneous Al distribution on the surface of LLZO particles has been reported by Geiger et al. [30]. Differences in the way in which Al is incorporated into the LLZO structure or is retained in the intergranular space as a secondary phase may lead to variations in leaching behavior. The results of this study indicate that this difference in Al incorporation has a greater effect on leaching than the material being calcined or sintered. It is assumed that calcined LLZO #1 contained only Al-substituted LLZO while the other two samples contained additional intergranular Al. However, high-resolution transmission electron microscopy measurements of LLZO are challenging and beyond the scope of this study. Nevertheless, a detailed crystal structure analysis could be an interesting aspect for future research.

The XRD patterns of the leaching residues obtained after water leaching show mainly cubic LLZO and Li_2CO_3 impurities (Figure 4). For sintered LLZO #2, protonated LLZO was also found (indicated by an arrow). For the calcined LLZO #1 sample, minimal secondary phases of $La_2Zr_2O_7$ as well as $La(AlO_3)$ phase are present. For the calcined LLZO #2 sample, more secondary phases are present. Due to the number of reflexes in LLZO and the limitations of the XRD measurements, the reflexes cannot be assigned to specific phases. Here, a mixture of precursors, such as La_2O_3, Ta_2O_5, and ZrO_2, could be among them but also $LiZrO_2$ and $La(AlO_3)$. In summary, the cubic LLZO structure is present in all samples after water leaching.

In summary, water offers the opportunity to selectively leach up to 57% Li and 44% Al from LLZO. The Al leaching efficiency may vary between different LLZO samples. However, this finding is of less importance since Al is only a minor component in LLZO. In addition, Al is a common impurity in leach solutions of conventional LIBs, and various separation options, such as precipitation and ion exchange, have already been investigated [42,43].

3.3. Leaching with Mineral Acids

Mineral acids, such as sulfuric acid and hydrochloric acid, are commonly used for the leaching of black mass from conventional LIBs with a liquid electrolyte. The best leaching results have been obtained at acid concentrations of 1.2–2.6 M for sulfuric acid and of

2.8–4.0 M for hydrochloric acid, S/L ratios of 50–150 g/L, temperatures of 60–80 °C, and leaching times of 1–2 h [21–23].
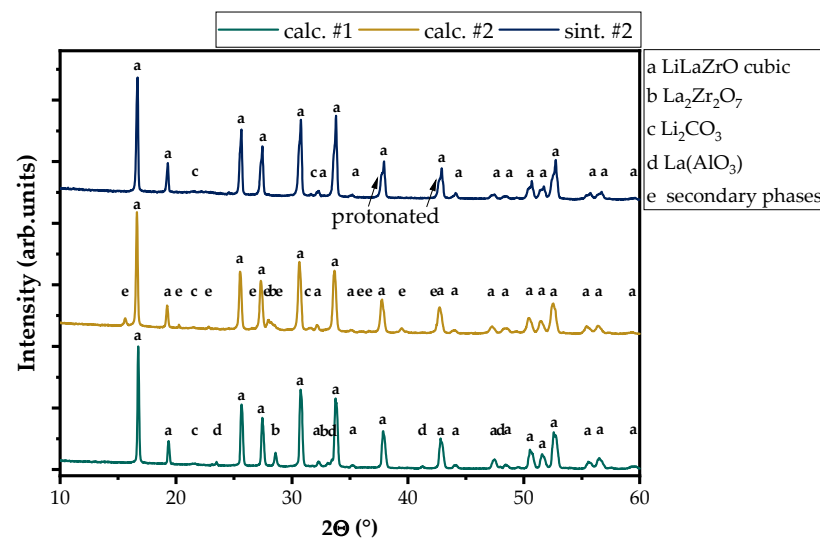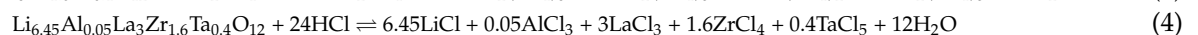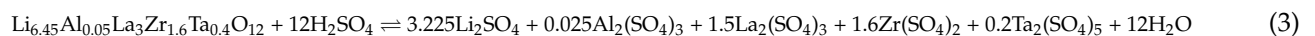

Figure 4. XRD patterns of leaching residues after 24 h leaching in water for calcined LLZO #1, calcined LLZO #2, and sintered LLZO #2. The present phases are cubic LLZO (ICSD: 182312), $La_2Zr_2O_7$ (ICSD: 015165), Li_2CO_3 (ICSD: 066941), and $La(AlO_3)$ (ICSD: 090538).

Theoretical considerations suggest that strong acids at elevated temperatures are required to leach sintered LLZO [27]. The first experimental investigations with garnet-type $Li_5La_3Nb_2O_{12}$ [38] and $Li_{6.25}Al_{0.25}La_3Zr_2O_{12}$ [28] confirmed that hydrochloric acid is a suitable leaching agent. Therefore, this study explored these commonly used mineral acids as lixiviants for the leaching of LLZO solid electrolyte. The following chemical reactions are proposed for the leaching of stoichiometric Al- and Ta-substituted LLZO in sulfuric acid (Equation (3)) and hydrochloric acid (Equation (4)):

$$Li_{6.45}Al_{0.05}La_3Zr_{1.6}Ta_{0.4}O_{12} + 12H_2SO_4 \rightleftharpoons 3.225Li_2SO_4 + 0.025Al_2(SO_4)_3 + 1.5La_2(SO_4)_3 + 1.6Zr(SO_4)_2 + 0.2Ta_2(SO_4)_5 + 12H_2O \quad (3)$$

$$Li_{6.45}Al_{0.05}La_3Zr_{1.6}Ta_{0.4}O_{12} + 24HCl \rightleftharpoons 6.45LiCl + 0.05AlCl_3 + 3LaCl_3 + 1.6ZrCl_4 + 0.4TaCl_5 + 12H_2O \quad (4)$$

In our study, almost complete dissolution of LLZO is achieved with 1 M sulfuric acid and 1 M hydrochloric acid at room temperature, as shown in Figure 5. Leaching efficiencies do not change significantly between 3 and 24 h for sulfuric acid but increase by up to 10% for hydrochloric acid. In general, the calcined and sintered LLZO samples show similar leaching behavior. The largest deviation was observed for Al, which could be due to the variation in Al incorporation (see Section 3.2). Due to the almost complete leaching of LLZO in the mineral acids, the leaching residues were not subjected to phase analysis.

Our results are in agreement with previously published studies [28,38]. Strong mineral acids are effective lixiviants for the complete dissolution of LLZO. Furthermore, it was shown that high leaching efficiencies can be achieved at low acid concentrations within 3 h at room temperature.

3.4. Leaching with Organic Acids

Organic acid leaching is gaining increasing attention in battery recycling because organic acids are biodegradable, can reduce process emissions, and can improve leaching by metal complexation. In general, organic acids with a higher number of carboxyl groups show better leaching efficiencies due to the higher stability of the metal complexes formed. In addition, some organic acids have special properties. These include, among others, formic acid, which can act as a reducing agent, and oxalic acid, which can form metal precipitates that allow for selective leaching. Due to the large number of organic acids, the optimal leaching conditions for black mass obtained from conventional LIBs are

diverse [24–26]. To the best of the authors' knowledge, there is no study on LLZO leaching with organic acids available.
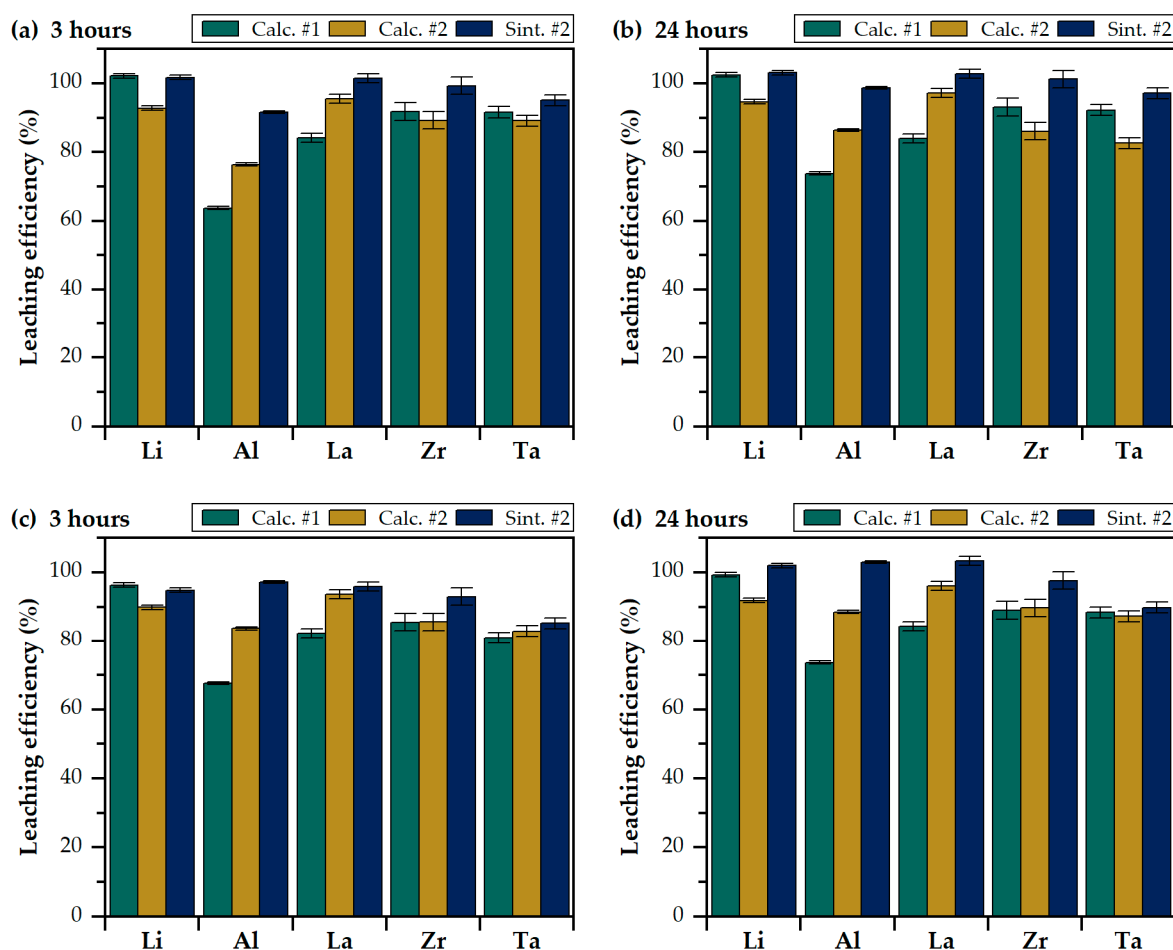

Figure 5. Leaching efficiencies of the calcined and sintered LLZO samples in sulfuric acid after 3 h (**a**) and 24 h (**b**) and in hydrochloric acid after 3 h (**c**) and 24 h (**d**) (acid concentration = 1 M, S:L ratio = 50 g/L, and T = 25 °C).

For this leaching study, we selected monocarboxylic acetic acid and formic acid, dicarboxylic oxalic acid, and tricarboxylic citric acid as lixiviants. Many metal complexes can be formed with the various organic acids studied. Stability constants for the individual metal complexes can be found in the literature [44–46]. The organic acid leaching results of the calcined and sintered LLZO samples after 3 h and 24 h are shown in Figure 6. To verify the phases present after LLZO leaching, XRD analyses were performed on the residues obtained after leaching for 24 h (Figure 7). The results of the individual acids are presented and discussed in the following section.
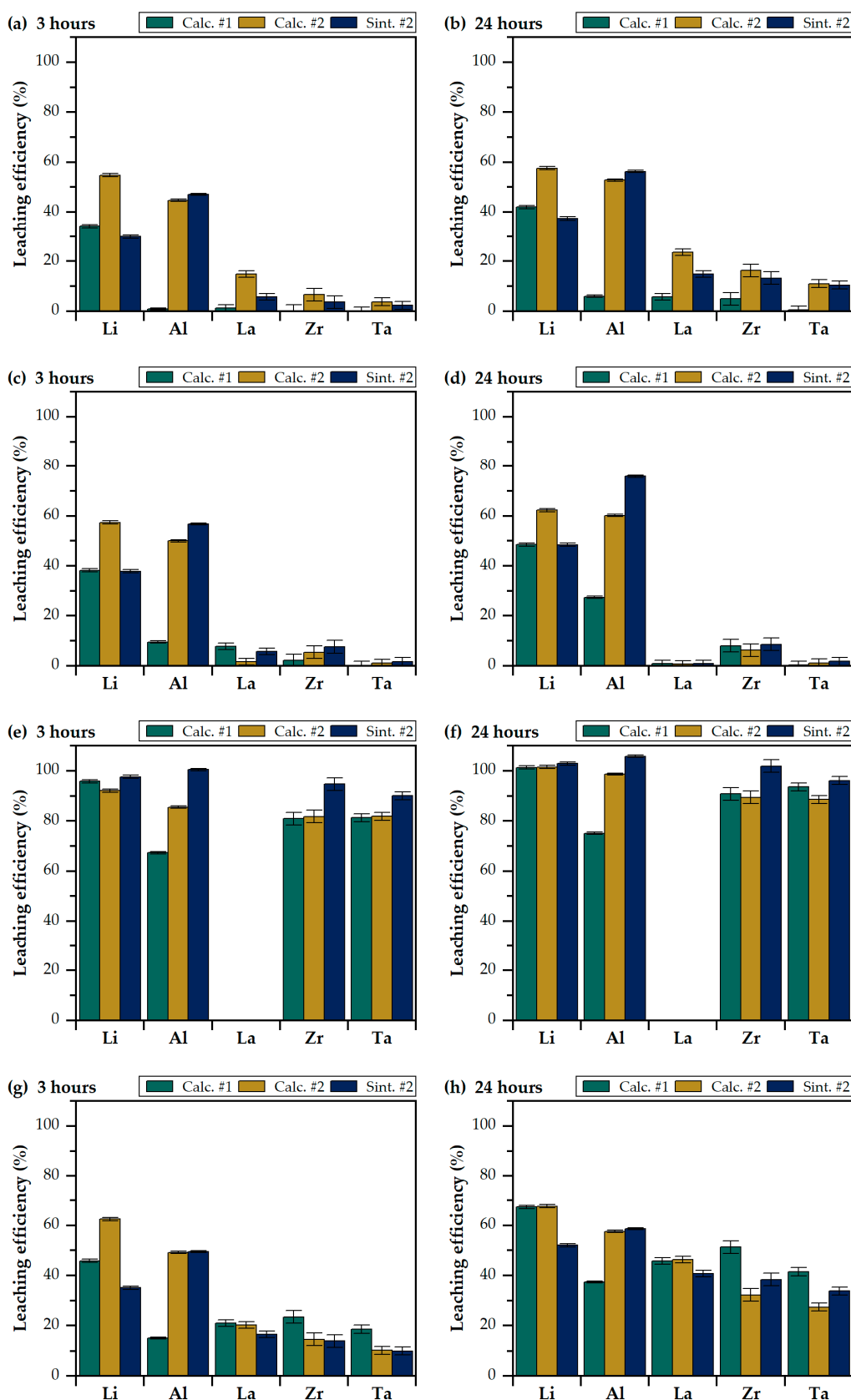
Figure 6. Leaching efficiencies of the calcined and sintered LLZO samples with organic acids: acetic acid (**a**,**b**), formic acid (**c**,**d**), oxalic acid (**e**,**f**), and citric acid (**g**,**h**) (acid concentration = 1 M, S:L ratio = 50 g/L, and T = 25 °C). The largest deviation in leaching efficiency was observed for Al, which could be due to an inhomogeneous Al distribution within the samples (see Section 3.2).
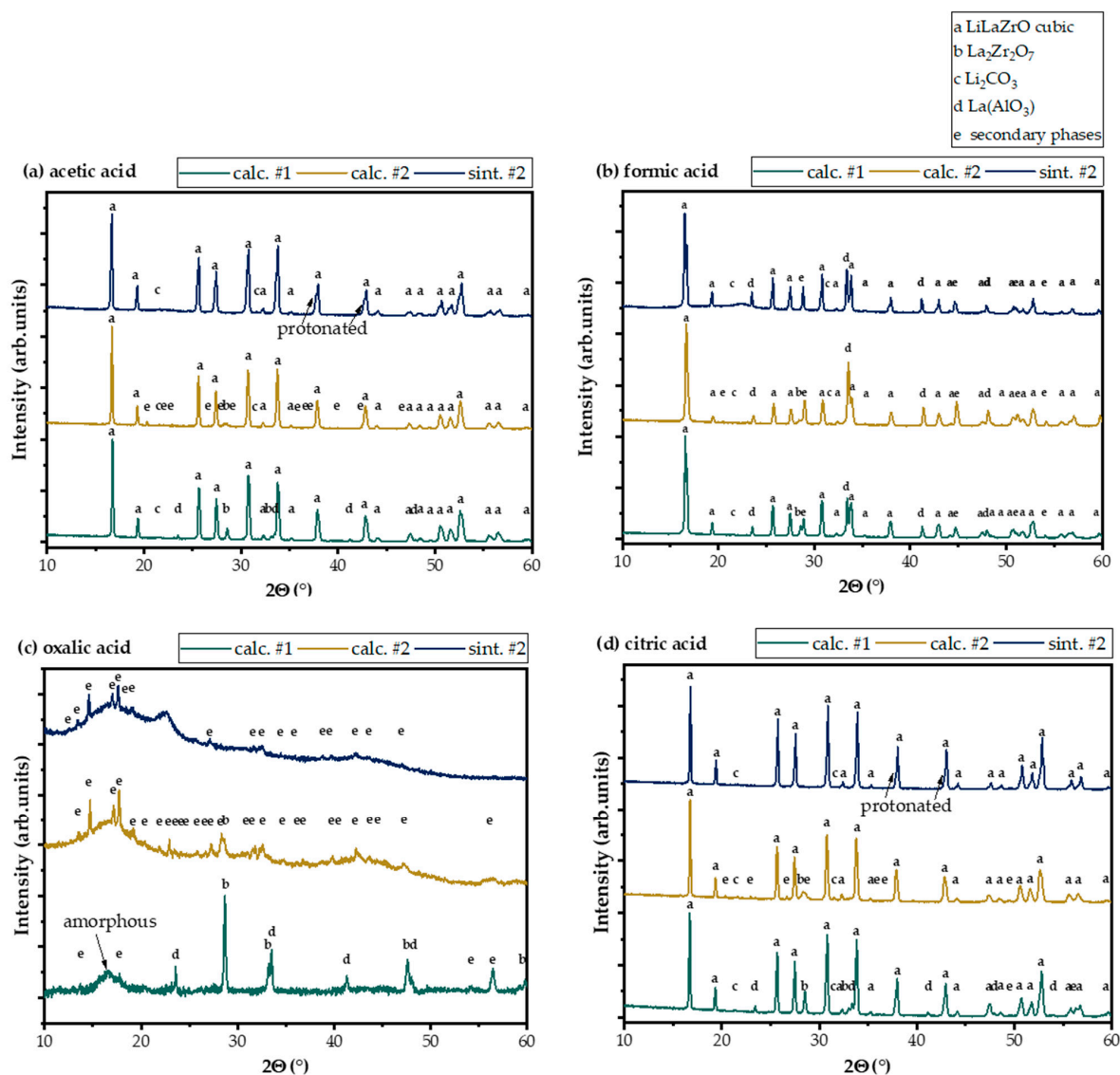
a LiLaZrO cubic
b La$_2$Zr$_2$O$_7$
c Li$_2$CO$_3$
d La(AlO$_3$)
e secondary phases

Figure 7. XRD patterns of leaching residues after 24 h of the calcined and sintered LLZO samples with organic acids: acetic acid (**a**), formic acid (**b**), oxalic acid (**c**), and citric acid (**d**). the present phases are cubic LLZO (ICSD: 182312), La$_2$Zr$_2$O$_7$ (ICSD: 015165), Li$_2$CO$_3$ (ICSD: 066941), and La(AlO$_3$) (ICSD: 090538).

Among the organic acids studied, monocarboxylic acetic and formic acid achieved the lowest leaching efficiencies (Figure 6a–d). Compared to the other constituents, Li and Al had the highest leaching efficiencies. Formic acid had slightly higher Li and Al leaching efficiencies than acetic acid. For example, the average Li leaching efficiencies were 53% in formic acid and 46% in acetic acid after 24 h of leaching. La, Zr, and Ta achieved low leaching efficiencies of less than 20%. The measured leaching efficiencies were supported by the XRD analyses of the leaching residues (Figure 7a,b). Cubic LLZO as the main phase and Li$_2$CO$_3$ impurities were present in all leaching residues obtained after leaching with acetic acid and formic acid. A small amount of La(AlO$_3$) was found in the residue of the calcined LLZO #1 sample leached with acetic acid and in all residues leached with formic acid. La$_2$Zr$_2$O$_7$ was found in the calcined LLZO residues for both acids. In addition, secondary phases were found in all residues of formic acid leaching (as described in Section 3.2). For acetic acid, only the residue of the calcined LLZO #2 sample showed secondary phases, as did the original sample before leaching. For the residue of the sintered LLZO #1 sample, a protonated LLZO phase was found when leached in acetic acid, as was the leaching

residue in water. Black mass leaching studies indicate a correlation between the leaching efficiencies of organic acids and their physicochemical properties such as acid strength, complexation ability, and stability of the complexes formed [25,47]. Our results for acetic acid and formic acid confirmed that these weak organic acids were not able to dissolve LLZO to a sufficient extent at the process parameters studied.

Dicarboxylic oxalic acid, a strong organic acid, showed high leaching efficiencies comparable to the mineral acids, except for La (Figure 6e,f). La probably precipitated as La oxalate, which could not be confirmed by XRD due to the low sample crystallinity (Figure 7c) [48]. Most of the reflections were assigned to different La-rich phases, indicating the formation of La oxalate, but this could not be fully determined at this point. Cubic LLZO was no longer detected, and only minorities of the secondary phase $La_2Zr_2O_7$ were present, as shown by the low crystallinity of the residues. However, a calcination step at 800 °C could produce crystalline La_2O_3 for resynthesis [49]. These results show that a selective removal of La is possible during the leaching process, which simplifies the further separation and purification process.

Tricarboxylic citric acid, a medium-strong organic acid, had the second-highest leaching efficiency of the four organic acids studied (Figure 6g,h). Unlike acetic acid and formic acid, citric acid also leached up to 50% of La, Zr, and Ta in 24 h. Cubic LLZO was the main phase of the remaining leaching residues from both the calcined and sintered LLZO samples. Small amounts of $La_2Zr_2O_7$ were identified only in the calcined LLZO residues, and small amounts of $La(AlO_3)$ were identified in the residue of the calcined LLZO #1 sample. In addition, secondary phases were present in the calcined LLZO residues (as described in Section 3.2). Based on the results, citric acid may be suitable for complete dissolution of LLZO if leaching conditions are optimized.

For future LLZO leaching studies, oxalic acid offers interesting possibilities for the selective recovery of La. Citric acid may be an alternative to strong mineral acids for a complete dissolution of LLZO. Although different secondary phases were observed in the leaching residues, the cubic LLZO phase was still the main phase. This was true for all organic acids studied except oxalic acid, where low crystalline La-rich phases were detected.

3.5. Assessment of Lixiviants

A unique aspect of this investigation was the holistic acid screening approach of LLZO solid electrolyte, making the study highly relevant for the development of flexible hydrometallurgical recycling processes for future LIB generations. To evaluate the investigated lixiviants, their technical performance was assessed using the following parameters:

- CRM leaching efficiency Y_{CRM}: a measure of Li, La, and Ta leaching efficiencies after 24 h normalized to 100%;
- Li selectivity S_{Li}: a measure of how selectively a lixiviant transfers Li into the leach solution after 24 h of leaching (≤ 1 unselective, >1 selective);
- La selectivity S_{La}: a measure of how selectively a lixiviant transfers La into the leach solution—or the residue if La is not leached—after 24 h of leaching (≤ 1 unselective, >1 selective);
- Increase in leaching efficiency ΔY: average increase in leaching efficiencies of all elements analyzed from 3 to 24 h, weighted according to the chemical composition of the feed (<1—decrease in leaching efficiency, 1—no change in leaching efficiency, and >1—increase in leaching efficiency);
- Share of residue after leaching $w_{residue}$: a measure of the proportion of the solid residue in relation to the initial sample weight.

The results are shown in Table 2. The values highlighted in red are unfavorable, the values in yellow are neutral, and the values in green are favorable. The equations used to calculate the parameters are presented in Supplementary Material S5.

Table 2. Assessment of the different lixiviants investigated for LLZO leaching shown as a heatmap (green—favorable, yellow—neutral, and red—unfavorable).

Lixiviant	CRM Leaching Efficiency (%)	Li Selectivity (-)	La Selectivity (-)	Increase of Leaching Efficiency (-)	Share of Residue after Leaching (wt%)
Water	13.9	2.5	1.2 [1]	1.0	86.4
Sulfuric acid	95.1	1.1	1.0	1.0	3.4
Hydrochloric acid	93.6	1.0	1.0	1.0	4.7
Acetic acid	22.6	1.7	0.6	5.7	76.7
Formic acid	18.3	2.0	1.3 [1]	0.8	93.5
Oxalic acid	64.9	1.3	4.4 [1]	1.0	90.8
Citric acid	47.0	1.3	0.9	2.3	51.8

[1] The La selectivity was calculated for the residue because La was not leached with these lixiviants.

Sulfuric acid and hydrochloric acid achieved the highest CRM leaching efficiencies in this study, resulting in an almost complete dissolution of LLZO. Since leaching with these two mineral acids is not selective for Li or La, a multi-stage purification and separation process is required. Sulfuric acid is a cheap and commonly used lixiviant in conventional LIB recycling processes. Furthermore, sulfuric acid is less corrosive and less fuming than hydrochloric acid. Therefore, LLZO leaching with sulfuric acid should be further investigated. The use of sulfuric acid could lead to flexible recycling processes of current LIB generations being adapted to SSBs.

Despite having the lowest CRM leaching efficiency, water was the most selective lixiviant for Li. The leaching reaction was considered complete after only 3 h, as no increase in leaching efficiency was observed during the remainder of the experiment. Water could be used in the first leaching stage of a hydrometallurgical SSB recycling process. Early in the process, a significant amount of Li could be transferred to the solution and subsequently recovered. Additionally, as investigated for conventional LIBs [50], early-stage Li recovery is of particular interest as Li losses typically occur along the process chain. Moreover, water is a cheap and non-hazardous lixiviant. The first leaching stage with water could be followed by a second leaching stage with a strong acid. Based on the results of this study, a two-staged leaching process using water and sulfuric acid would result in overall leaching efficiencies of 100% for Li and Al, 95% for La, 94% for Zr, and 91% for Ta.

The CRM leaching efficiencies of the organic acids ranged between those of water and those of the mineral acids. Acetic acid and formic acid selectively leached Li. However, these acids are not suitable as selective lixiviants for Li because they also leached a small amount of the other elements. As a result, Li could not be extracted directly from the leach solution, and the solution would have to be purified first. The CRM leaching efficiency of citric acid was 47%, and the leaching efficiency more than doubled from 3 to 24 h. Since the study was conducted at a low acid concentration and room temperature, there is potential to optimize the process parameters. Therefore, citric acid could be an alternative to sulfuric acid for the complete dissolution of LLZO. Oxalic acid had a very high CRM leaching efficiency of 64.9%, considering that La was almost quantitatively precipitated from the leach solution. Therefore, oxalic acid offers interesting possibilities for the selective recovery of La during leaching, which should be further investigated.

The results of this fundamental study on LLZO leaching indicate that sulfuric acid, and possibly citric acid, could be suitable lixiviants to dissolve LLZO with high leaching efficiencies in a single leaching step. Oxalic acid could be used as a selective lixiviant to recover La as oxalate already during leaching. Water could be used as a selective lixiviant for Li in a two-staged leaching process. These results lead to the two different process approaches for LLZO leaching shown in Figure 8: either complete LLZO dissolution or selective two-staged LLZO leaching.
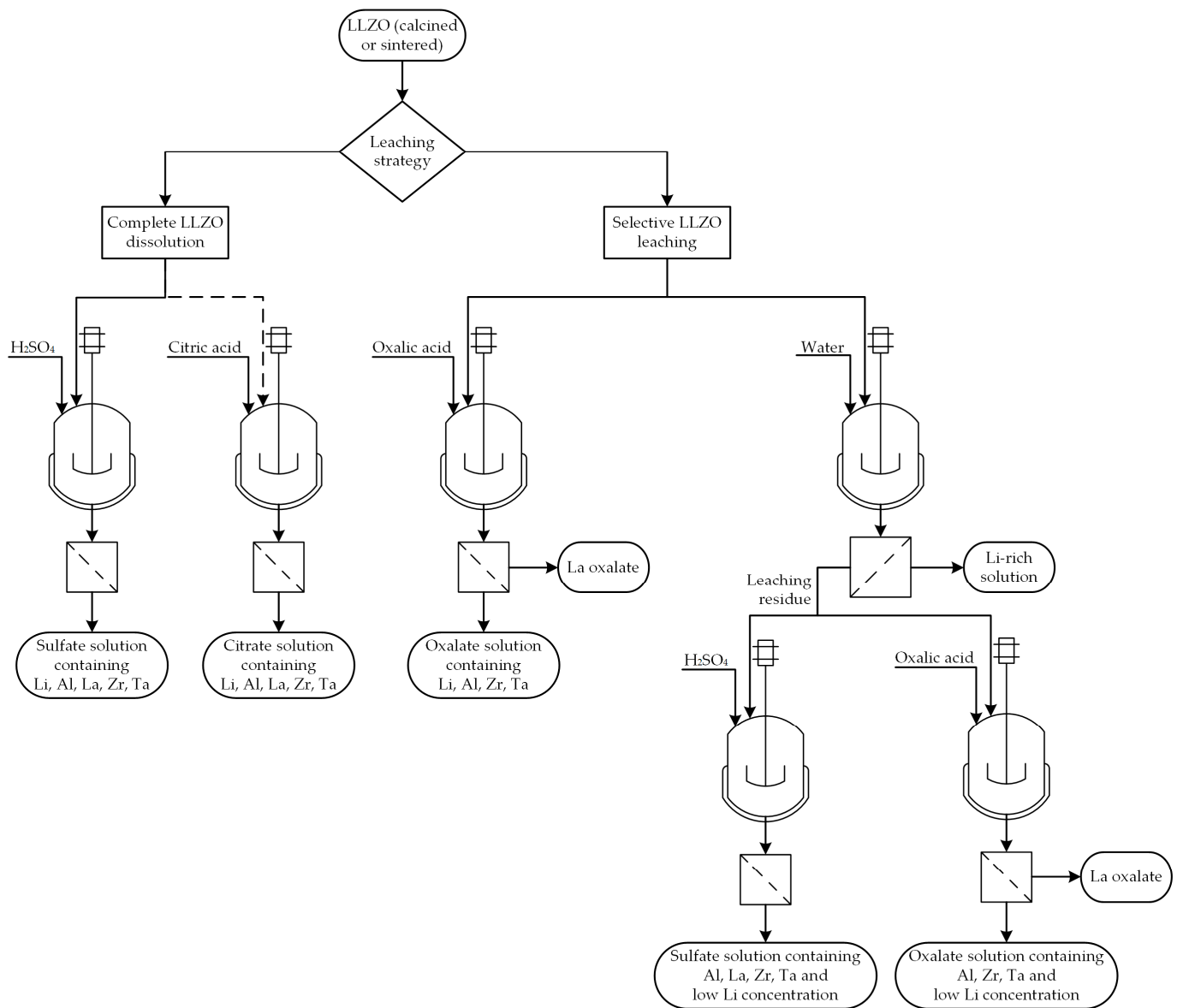
Figure 8. Process approaches for LLZO leaching based on the results of this study. Leaching with citric acid is shown with a dashed line, as the process parameters will need to be optimized for complete dissolution of LLZO.

When transferring the obtained fundamental results to SSB cells, a life-cycle engineering approach will be required, taking into account not only the technical but also the environmental and economic impacts.

4. Conclusions

This study fills the current knowledge gap on hydrometallurgical recycling of next-generation SSBs containing Al- and Ta-substituted LLZO. By providing new insights into the leaching behavior of LLZO, the results will assist in the selection of suitable leaching strategies for hydrometallurgical recycling. Since SSB production wastes from the ramp-up of industrial production are the first expected material flows for future recycling processes, this study presents a holistic acid screening with actual LLZO production wastes. The results promote the development of flexible recycling routes with options for complete and selective LLZO dissolution.

The experimental results show that LLZO is almost completely dissolved in strong acids under the mild process conditions investigated. Sulfuric acid and hydrochloric acid

almost completely dissolved LLZO with leaching efficiencies above 90%. Since sulfuric acid is a cheap and commonly used lixiviant in conventional LIB recycling processes, the use of sulfuric acid could lead to such recycling processes being adapted to SSBs. Oxalic acid also almost completely dissolved LLZO, but it simultaneously precipitated La as oxalate, with leaching efficiencies above 92% for the other elements. The use of oxalic acid allows La to be separated from the other elements early in the process and makes the subsequent purification process less complex.

A possible selective LLZO leaching approach consisting of a two-staged leaching process could be pursued with water and a strong acid. It was demonstrated that up to 57% of Li was selectively leached with water. When LLZO is first leached in water, a significant amount of Li could be transferred to the solution and subsequently recovered early in the process. Early-stage Li recovery is of particular interest because Li losses typically occur along the process chain. According to our results, the proposed two-staged leaching process using water and sulfuric acid could result in overall leaching efficiencies of 100% for Li and Al, 95% for La, 94% for Zr, and 91% for Ta.

The experimental results provide vital knowledge for the development of highly efficient recycling processes for SSBs containing LLZO. After further process insights have been gained through LLZO leaching optimization experiments, it should be determined whether the test parameters found for pure LLZO can be transferred to mechanically processed SSB cells that also contain electrode-active materials.

Supplementary Materials: The following supporting information can be downloaded at https://www.mdpi.com/article/10.3390/met13050834/s1. S1: LLZO powder synthesis; S2: Thermal treatment of aged calcined LLZO; S3: Sintered LLZO pellets; S4: Elemental concentration of the pregnant leach solutions; S5: Calculations for the assessment of lixiviants; Figure S1: Thermal treatment of calcined LLZO #1 at 750 °C for 4 h under air atmosphere; Figure S2: Sintered LLZO #2 before grinding; Table S1: Elemental concentration of the pregnant leach solutions after 24 h of leaching.

Author Contributions: K.S. conceived and conducted the experiment(s). The materials were provided by V.K. and M.F. The crystallographic characterizations were executed by V.K. K.S. and B.Y. analyzed the experimental results. K.S., B.Y. and V.K. prepared the original draft. K.S., B.Y., V.K., M.F. and D.G. reviewed and edited the manuscript. All authors have read and agreed to the published version of the manuscript.

Data Availability Statement: The data presented in this study are available from the corresponding author upon reasonable interest.

Conflicts of Interest: The authors declare no conflict of interest.

References

1. Smalley, R.E. Future Global Energy Prosperity: The Terawatt Challenge. *MRS Bull.* **2005**, *30*, 412–417. [CrossRef]
2. Badwal, S.P.S.; Giddey, S.S.; Munnings, C.; Bhatt, A.I.; Hollenkamp, A.F. Emerging electrochemical energy conversion and storage technologies. *Front. Chem.* **2014**, *2*, 79. [CrossRef]
3. Nagaura, T. Lithium Ion Rechargeable Battery. *Prog. Batter. Sol. Cells* **1990**, *9*, 209–217.
4. Janek, J.; Zeier, W.G. A solid future for battery development. *Nat. Energy* **2016**, *1*, 16141. [CrossRef]

5. Pillot, C. EU Battery Demand and Supply (2019–2030) in a Global Context. Available online: https://www.eurobat.org/wp-content/uploads/2021/05/Avicenne_EU_Market_-_summary_110321.pdf (accessed on 28 January 2023).

6. RECHARGE Battery Industry Association. Battery Market and Technologies. Available online: https://rechargebatteries.org/battery-market-and-technologies/ (accessed on 28 January 2023).

7. Zhang, Y.S.; Schneider, K.; Qiu, H.; Zhu, H.L. A perspective of low carbon lithium-ion battery recycling technology. *Carbon Capture Sci. Technol.* **2022**, *5*, 100074. [CrossRef]

8. Nigl, T.; Baldauf, M.; Hohenberger, M.; Pomberger, R. Lithium-Ion Batteries as Ignition Sources in Waste Treatment Processes-A Semi-Quantitate Risk Analysis and Assessment of Battery-Caused Waste Fires. *Processes* **2021**, *9*, 49. [CrossRef]

9. Duan, J.; Tang, X.; Dai, H.; Yang, Y.; Wu, W.; Wei, X.; Huang, Y. Building Safe Lithium-Ion Batteries for Electric Vehicles: A Review. *Electrochem. Energ. Rev.* **2020**, *3*, 1–42. [CrossRef]

10. Murugan, R.; Thangadurai, V.; Weppner, W. Fast lithium ion conduction in garnet-type $Li_7La_3Zr_2O_{12}$. *Angew. Chem. Int. Ed* **2007**, *46*, 7778–7781. [CrossRef]

11. Gonzalez Puente, P.M.; Song, S.; Cao, S.; Rannalter, L.Z.; Pan, Z.; Xiang, X.; Shen, Q.; Chen, F. Garnet-type solid electrolyte: Advances of ionic transport performance and its application in all-solid-state batteries. *J. Adv. Ceram.* **2021**, *10*, 933–972. [CrossRef]

12. Balaish, M.; Gonzalez-Rosillo, J.C.; Kim, K.J.; Zhu, Y.; Hood, Z.D.; Rupp, J.L.M. Processing thin but robust electrolytes for solid-state batteries. *Nat. Energy* **2021**, *6*, 227–239. [CrossRef]

13. Takada, K. Progress in solid electrolytes toward realizing solid-state lithium batteries. *J. Power Source* **2018**, *394*, 74–85. [CrossRef]

14. Schneider, K.; Goldmann, D. Oxide-based lithium solid-state batteries from a recycling perspective. In Proceedings of the 16. Recy & DepoTech-Konferenz, Leoben, Austria, 9–11 November 2022; Pomberger, R., Ed.; Abfallverwertungstechnik & Abfallwirtschaft Eigenverlag. pp. 381–386.

15. Blengini, G.A.; El Latunussa, C.; Eynard, U.; Torres de Matos, C.; Wittmer, D.M.A.G.; Georgitzikis, K.; Pavel, C.C.; Carrara, S.; Mancini, L.; Unguru, M.; et al. *Study on the EU's List of Critical Raw Materials (2020): Final Report*; Publications Office of the European Union: Luxembourg, 2020; ISBN 978-92-76-21049-8.

16. Harper, G.; Sommerville, R.; Kendrick, E.; Driscoll, L.; Slater, P.; Stolkin, R.; Walton, A.; Christensen, P.; Heidrich, O.; Lambert, S.; et al. Recycling lithium-ion batteries from electric vehicles. *Nature* **2019**, *575*, 75–86. [CrossRef]

17. Doose, S.; Mayer, J.K.; Michalowski, P.; Kwade, A. Challenges in Ecofriendly Battery Recycling and Closed Material Cycles: A Perspective on Future Lithium Battery Generations. *Metals* **2021**, *11*, 291. [CrossRef]

18. Brückner, L.; Frank, J.; Elwert, T. Industrial Recycling of Lithium-Ion Batteries—A Critical Review of Metallurgical Process Routes. *Metals* **2020**, *10*, 1107. [CrossRef]

19. Nasser, O.A.; Petranikova, M. Review of Achieved Purities after Li-ion Batteries Hydrometallurgical Treatment and Impurities Effects on the Cathode Performance. *Batteries* **2021**, *7*, 60. [CrossRef]

20. Gupta, C.K.; Mukherjee, T.K. *Hydrometallurgy in Extraction Processes*; CRC Press: Boca Raton, FL, USA, 1990; ISBN 0849368049.

21. Neumann, J.; Petranikova, M.; Meeus, M.; Gamarra, J.D.; Younesi, R.; Winter, M.; Nowak, S. Recycling of Lithium-Ion Batteries—Current State of the Art, Circular Economy, and Next Generation Recycling. *Adv. Energy Mater.* **2022**, *12*, 2102917. [CrossRef]

22. Windisch-Kern, S.; Gerold, E.; Nigl, T.; Jandric, A.; Altendorfer, M.; Rutrecht, B.; Scherhaufer, S.; Raupenstrauch, H.; Pomberger, R.; Antrekowitsch, H.; et al. Recycling chains for lithium-ion batteries: A critical examination of current challenges, opportunities and process dependencies. *Waste Manag.* **2022**, *138*, 125–139. [CrossRef]

23. Larouche, F.; Tedjar, F.; Amouzegar, K.; Houlachi, G.; Bouchard, P.; Demopoulos, G.P.; Zaghib, K. Progress and Status of Hydrometallurgical and Direct Recycling of Li-Ion Batteries and Beyond. *Materials* **2020**, *13*, 801. [CrossRef]

24. Golmohammadzadeh, R.; Faraji, F.; Rashchi, F. Recovery of lithium and cobalt from spent lithium ion batteries (LIBs) using organic acids as leaching reagents: A review. *Resour. Conserv. Recycl.* **2018**, *136*, 418–435. [CrossRef]

25. Li, L.; Dunn, J.B.; Zhang, X.X.; Gaines, L.; Chen, R.J.; Wu, F.; Amine, K. Recovery of metals from spent lithium-ion batteries with organic acids as leaching reagents and environmental assessment. *J. Power Source* **2013**, *233*, 180–189. [CrossRef]

26. Okonkwo, E.G.; Wheatley, G.; He, Y. The role of organic compounds in the recovery of valuable metals from primary and secondary sources: A mini-review. *Resour. Conserv. Recycl.* **2021**, *174*, 105813. [CrossRef]

27. Schwich, L.; Küpers, M.; Finsterbusch, M.; Schreiber, A.; Fattakhova-Rohlfing, D.; Guillon, O.; Friedrich, B. Recycling Strategies for Ceramic All-Solid-State Batteries-Part I: Study on Possible Treatments in Contrast to Li-Ion Battery Recycling. *Metals* **2020**, *10*, 1523. [CrossRef]

28. Ali Nowroozi, M.; Iqbal Waidha, A.; Jacob, M.; van Aken, P.A.; Predel, F.; Ensinger, W.; Clemens, O. Towards Recycling of LLZO Solid Electrolyte Exemplarily Performed on LFP/LLZO/LTO Cells. *ChemistryOpen* **2022**, *11*, e202100274. [CrossRef]

29. Malkowski, T.F.; Boeding, E.D.; Fattakhova-Rohlfing, D.; Wettengl, N.; Finsterbusch, M.; Veith, G.M. Digestion processes and elemental analysis of oxide and sulfide solid electrolytes. *Ionics* **2022**, *28*, 3223–3231. [CrossRef]

30. Geiger, C.A.; Alekseev, E.; Lazic, B.; Fisch, M.; Armbruster, T.; Langner, R.; Fechtelkord, M.; Kim, N.; Pettke, T.; Weppner, W. Crystal chemistry and stability of "$Li_7La_3Zr_2O_{12}$" garnet: A fast lithium-ion conductor. *Inorg. Chem.* **2011**, *50*, 1089–1097. [CrossRef]

31. Buschmann, H.; Dölle, J.; Berendts, S.; Kuhn, A.; Bottke, P.; Wilkening, M.; Heitjans, P.; Senyshyn, A.; Ehrenberg, H.; Lotnyk, A.; et al. Structure and dynamics of the fast lithium ion conductor "$Li_7La_3Zr_2O_{12}$". *Phys. Chem. Chem. Phys.* **2011**, *13*, 19378–19392. [CrossRef]

32. *CRC Handbook of Chemistry and Physics: A Ready-Reference Book of Chemical and Physical Data*, 97th ed.; Haynes, W.M. (Ed.) CRC Press: Boca Raton, FL, USA; London, UK; New York, NY, USA, 2017; ISBN 9781498754293.

33. Rosen, M.; Ye, R.; Mann, M.; Lobe, S.; Finsterbusch, M.; Guillon, O.; Fattakhova-Rohlfing, D. Controlling the lithium proton exchange of LLZO to enable reproducible processing and performance optimization. *J. Mater. Chem. A* **2021**, *9*, 4831–4840. [CrossRef]

34. Ye, R.; Ihrig, M.; Imanishi, N.; Finsterbusch, M.; Figgemeier, E. A Review on Li^+/H^+ Exchange in Garnet Solid Electrolytes: From Instability against Humidity to Sustainable Processing in Water. *ChemSusChem* **2021**, *14*, 4397–4407. [CrossRef]

35. Cheng, L.; Crumlin, E.J.; Chen, W.; Qiao, R.; Hou, H.; Franz Lux, S.; Zorba, V.; Russo, R.; Kostecki, R.; Liu, Z.; et al. The origin of high electrolyte-electrode interfacial resistances in lithium cells containing garnet type solid electrolytes. *Phys. Chem. Chem. Phys.* **2014**, *16*, 18294–18300. [CrossRef]

36. Jin, Y.; McGinn, P.J. $Li_7La_3Zr_2O_{12}$ electrolyte stability in air and fabrication of a $Li/Li_7La_3Zr_2O_{12}/Cu_{0.1}V_2O_5$ solid-state battery. *J. Power Source* **2013**, *239*, 326–331. [CrossRef]

37. Sharafi, A.; Yu, S.; Naguib, M.; Lee, M.; Ma, C.; Meyer, H.M.; Nanda, J.; Chi, M.; Siegel, D.J.; Sakamoto, J. Impact of air exposure and surface chemistry on $Li–Li_7La_3Zr_2O_{12}$ interfacial resistance. *J. Mater. Chem. A* **2017**, *5*, 13475–13487. [CrossRef]

38. Truong, L.; Thangadurai, V. Soft-Chemistry of Garnet-Type $Li_{5+x}Ba_xLa_{3-x}Nb_2O_{12}$ (x = 0, 0.5, 1): Reversible $H^+ \leftrightarrow Li^+$ Ion-Exchange Reaction and Their X-ray, ^7Li MAS NMR, IR, and AC Impedance Spectroscopy Characterization. *Chem. Mater.* **2011**, *23*, 3970–3977. [CrossRef]

39. Liu, C.; Rui, K.; Shen, C.; Badding, M.E.; Zhang, G.; Wen, Z. Reversible ion exchange and structural stability of garnet-type Nb-doped $Li_7La_3Zr_2O_{12}$ in water for applications in lithium batteries. *J. Power Source* **2015**, *282*, 286–293. [CrossRef]

40. Yow, Z.F.; Oh, Y.L.; Gu, W.; Rao, R.P.; Adams, S. Effect of Li^+/H^+ exchange in water treated Ta-doped $Li_7La_3Zr_2O_{12}$. *Solid State Ion.* **2016**, *292*, 122–129. [CrossRef]

41. Cao, S.; Song, S.; Xiang, X.; Hu, Q.; Zhang, C.; Xia, Z.; Xu, Y.; Zha, W.; Li, J.; Gonzale, P.M.; et al. Modeling, Preparation, and Elemental Doping of $Li_7La_3Zr_2O_{12}$ Garnet-Type Solid Electrolytes: A Review. *J. Korean Ceram. Soc* **2019**, *56*, 111–129. [CrossRef]

42. Peng, F.; Mu, D.; Li, R.; Liu, Y.; Ji, Y.; Dai, C.; Ding, F. Impurity removal with highly selective and efficient methods and the recycling of transition metals from spent lithium-ion batteries. *RSC Adv.* **2019**, *9*, 21922–21930. [CrossRef]

43. Virolainen, S.; Wesselborg, T.; Kaukinen, A.; Sainio, T. Removal of iron, aluminium, manganese and copper from leach solutions of lithium-ion battery waste using ion exchange. *Hydrometallurgy* **2021**, *202*, 105602. [CrossRef]

44. Martell, A.E.; Smith, R.M. *Critical Stability Constants: Other Organic Ligands*; Springer: Boston, MA, USA, 1977; ISBN 978-1-4757-1570-5.

45. Martell, A.E. *Critical Stability Constants: Second Supplement*; Springer: New York, NY, USA, 1989; ISBN 9781461567646.

46. Martell, A.E. *Critical Stability Constants: First Supplement*; Springer: New York, NY, USA, 1982; ISBN 9781461567615.

47. Golmohammadzadeh, R.; Rashchi, F.; Vahidi, E. Recovery of lithium and cobalt from spent lithium-ion batteries using organic acids: Process optimization and kinetic aspects. *Waste Manag.* **2017**, *64*, 244–254. [CrossRef] [PubMed]

48. Kolthoff, I.M.; Elmquist, R. The solubilities of lanthanum oxalate and of lanthanum hydroxide in water. The mobility of the lanthanum ion at 25°. *J. Am. Chem. Soc.* **1931**, *53*, 1217–1225. [CrossRef]

49. Balboul, B.A.A.; El-Roudi, A.M.; Samir, E.; Othman, A.G. Non-isothermal studies of the decomposition course of lanthanum oxalate decahydrate. *Thermochim. Acta* **2002**, *387*, 109–114. [CrossRef]

50. Schwich, L.; Schubert, T.; Friedrich, B. Early-Stage Recovery of Lithium from Tailored Thermal Conditioned Black Mass Part I: Mobilizing Lithium via Supercritical CO_2-Carbonation. *Metals* **2021**, *11*, 177. [CrossRef]